Characterization of Nanoporous Materials

Leila Keshavarz, Mohammad Reza Ghaani, Omid Saremi, and Niall J. English

Abstract Nanoporous materials have aroused huge attention in research and development due to their capability in numerous areas such as gas storage, separation, and catalysis processes, membranes, microdevices, etc. The properties of nanoporous materials are controlled by the arrangement of atoms in the crystal as well as the specific surface area and porosity. Detailed information about textural properties, such as pore size, shape, surface morphology, and connectivity, and composition of nanoporous materials has a significant effect on their efficiency and performance, and therefore, it is necessary to determine their properties. The development of nanoporous materials featuring uniform, tailor-made pore structures, and offers the tremendous capability for these applications. In this respect, this chapter emphasizes and explains both existing and novel methods for the synthesis and characterization of nanoporous materials, which is essential to galvanize yet more progress in these materials' further development.

Keywords Nanoporous · Characterization · Crystalline structure · Oxidation state & coordination · Chemical composition · Pore analysis

1 Introduction

There is a wide variety of solid nanoporous materials, including nanoporous carbons, zeolites, nanoporous inorganic oxides, together with nanoporous polymers. With advances in fabricating nanoporous materials with tailor-made pore structures and with changing synthesis conditions, it is possible to control the size of these channels and their surface properties; excitingly, this offers huge potential for different applications. There is a great, renewed interest in the characterization of novel

L. Keshavarz (✉) · M. R. Ghaani · O. Saremi · N. J. English (✉)
School of Chemical and Bioprocess Engineering, University College Dublin, Belfield, Dublin 4, Ireland
e-mail: leila.keshavarz@ucd.ie

N. J. English
e-mail: niall.english@ucd.ie

A. Uthaman et al. (eds.), *Advanced Functional Porous Materials*, Engineering Materials,
https://doi.org/10.1007/978-3-030-85397-6_10

nanoporous materials, owing to impressive recent achievements in modern characterization methods. To produce a repeatable synthesis of nanomaterials, their characterization is rightly considered to be pivotal. Also, consideration of a detailed textual analysis of nanoporous materials is vital to acquiring precise information on, *inter alia*, the pore size, surface area, and network connectivity. Incorporation of this data with studies on process performance helps to coordinate the structural properties of materials with their performance for gas storage, separation, and catalytic processes. A variety of techniques with different degrees of uncertainty are available for the textural and structural characterization of nanoporous materials, such as gas adsorption, electron microscopy, nuclear magnetic resonance methods, X-ray analysis, and various spectroscopic methods (Senthil Kumar et al. 2019). Every technique has some advantages as well as limitations in application range. This chapter contains a brief description of different characterization methods and demonstrates their application to characterize the surface and structural properties of nanoporous material, while also summarizing recent progress in the field of nanoporous materials characterization; to do so, we adopt a nanoporous materials-characterization "categorization scheme" as depicted in Fig. 1.

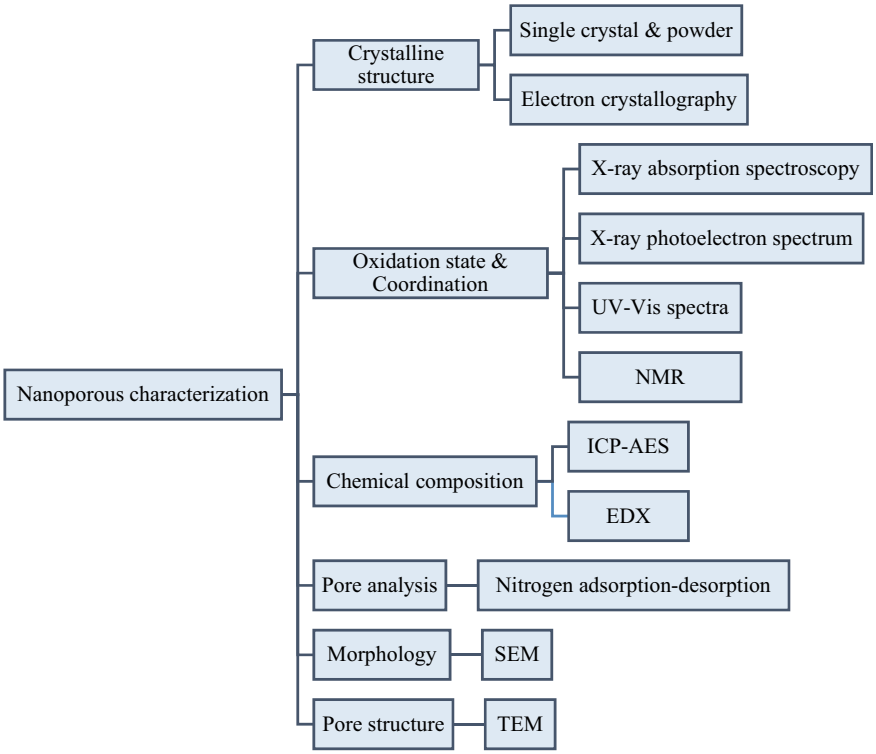

Fig. 1 Classification of characterization methods for nanoporous materials

2 Crystalline Structure

Usually, the structural resolution of porous materials is challenging as most porous materials are polycrystalline with complex featuring large unit cells, and the materials are indeed sometimes disordered. Moreover, the group of species included in the pores of the crystal cause more difficulty for the structure determination of nanoporous materials. Common solid nanoporous materials can be classified as polymeric, metals, carbon, aluminosilicate, and oxides (Fayed et al. 2016). Nanoporous materials have increased the domain of zeolites, and new nanoporous materials developed such as new porous metal-organic frameworks (MOFs) and coordination polymers (PCPs), porous metalophosphates, and hybrid materials. Consequently, new challenges are facing for the structural characterization of these nanoporous crystals. To determine the structure of nanoporous materials, it is of paramount importance to determine the periodic arrangement of the material within the bulk of the crystal and averaged structures and then probe the structural deflection from perfect infinite crystal, such as surface- and defect-based fine structures, as well as incommensurate structures. As reported by the International Union of Pure and Applied Chemistry (IUPAC), there are three categories of nanoporous materials: micropores (pore sizes < 2 nm), mesoporous (2–50 nm), and macrospores (>50 nm). A comparison of these different pore systems of mesoporous is shown in Fig. 2 (Fayed et al. 2016).

For example, MOF structures (Helliwell et al. 2008) have pores of uniform size up to 3 nm containing metal salts as the inorganic source, together with organic molecules featuring O or N donor atoms. For finding the framework structure of this nanoporous material, the challenge lays first in detecting the non-framework groups, including template molecules. The next step that is more challenging is finding the location of the site(s) of the replaced metal atoms and the acidic sites. However, during the production of these materials formed by heating the "as-synthesized" materials, it is necessary to consider changes that occurred especially the oxidation state changes of the incorporated metal atoms.

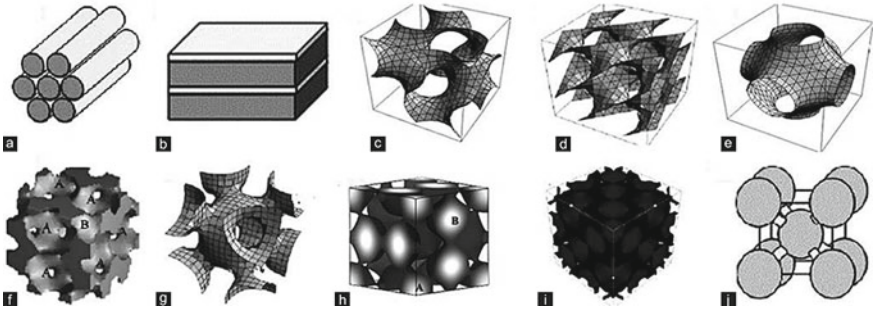

Fig. 2 Various structures of mesoporous silicates, **a** 2D-hexagonal, **b** lamellar, **c** Ia-3d, **d** Pn-3 m, **e** Im-3, **f** Pm-3n, **g** Fm-3 m, **h** Im-3 m, **i** Fd-3 m and **j** body-centered cubic structures (reproduced, with permission, from Fayed et al. 2016)

Among the existing structure determination tools, single-crystal and powder X-ray diffraction and electron crystallography are the most common characterization methods for the crystalline structure of nanoporous materials (Liu et al. 2013). Distance ordered-arrangement of pores could be measured by electron crystallography (EC). Single-crystal XRD (SXRD) is a non-destructive analytical technique and enables detailed information about the crystal, such as cell dimension, bond length, bond angle, etc. Powder X-ray diffraction (PXRD) is another technique applied to determine the crystallographic analysis of a powder sample.

2.1 Single Crystal and Powder XRD

X-ray diffraction (XRD) technique is among the common techniques for characterization of the long-range order in materials including nanoporous materials. XRD is a quick, non-destructive analysis of multicomponent mixtures that provides information regarding the microstructure of 3D crystalline structure (including grain size, lattice constant, and strains, nature of the phase), without the need for extensive sample preparation. The diffraction pattern achieved from the XRD analysis provides a sharp and considerable peak for the crystalline compound.

W. L. Bragg proposed that when X-ray incident onto a crystal surface, the interaction of X-rays defined based on the reflection from crystal planes, which is called Bragg's Law (Bragg and Bragg 1913):

$$n\lambda = 2d \sin\theta \tag{1}$$

Here θ is the angle of the incident X-ray beam, d is the spacing of the crystal layers (path difference), λ is the wavelength of the incident beam, and n is a constant.

In the constant wavelength, Bragg's law expresses that the angles of X-rays reflect by a set of lattice planes only depending on the d-spacing. In Fig. 3, two sets of reflections from the A and B planes which reflect at the same angle are different in

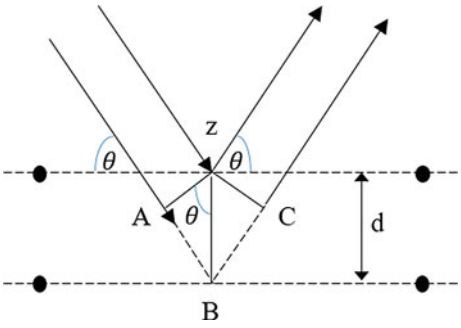

Fig. 3 Reflection of X-rays beam from two lattice planes attributed to the family $H \equiv (h, k, l)$

phase depending on d, λ, and they are different in amplitude if they are not from the same atoms (Martis 2011).

Single-Crystal X-Ray Diffraction

The most feasible and well-established technique for characterization of crystalline materials and understanding the atomic arrangement is single-crystal X-ray diffraction (SXRD). Generally, larger crystals of nanoporous material are suitable for characterization by SXRD. The angles and intensities of X-ray diffraction apply to generate a 3D image of the density of electrons, which reflects the average positions of atoms in the crystal. Three-dimensional XRD intensity data from a single crystal require approximately less than 10 h. This method has some limitations, in that when the crystals are too small. Therefore, the main difficulty of structure determination by SXRD lies in the crystal size itself, despite the brightest synchrotron light sources needing to be at least a few micrometers.

In the case of nanoporous materials, SXRD has been applied to determine the structure of various open-framework oxides and metal-organic frameworks, as it is relatively easy to form crystals large enough for SXRD of such materials (Kaskel 2017). Contrarily, this method is not very popular for zeolites, and only a limited number of zeolites have been solved by SXRD. High internal stress during solvent removal of nanoporous materials tends to induce cracking in single crystals. Therefore, crystal fragmentation and defect formation of nanoporous materials can be often caused by desolvation, none of which is favorable for SXRD studies. Another challenge explaining the paucity of such studies in the literature centers on the inherent difficulty in carrying out structure determination of disordered crystals. Moreover, some nanoporous materials are usually isolated as microcrystalline powders, and resultant structures are mainly determined from powder-XRD data.

Halder and Kerpet developed a novel in situ SXRD technique to ascertain, as a function of temperature and vapor pressure which enables continuous monitoring of the single-crystal structure during the desorption and adsorption of different guest species into a porous coordination framework (Halder and Kepert 2005). In this method, mechanisms of structural rearrangements of the framework, together with desirable adsorption sites for gases, can be determined at the same time. Structure modeling can also be performed by XRD diffraction patterns using various software (e.g., TOPAS, Materials Studio), in conjunction with the Scherrer-equation treatment of broadening of the most intense peak of XRD measurements for specific samples.

When nanoporous single-crystal growth is difficult, structure solution from powder-diffraction data itself can be achieved.

Powder X-Ray Diffraction

This technique can be applied to determine information for crystalline materials and periodically arranged clusters, such as, *inter alia*, phase identification, phase quantification, percent crystallinity, lattice-parameter refinement, Rietveld refinement, expansion tensors and bulk modulus, crystallite size, and strain. The 2D diffraction pattern illustrates concentric rings of scattering peaks refer to the different d spacings in the crystal lattice because the nanoscale powder is randomly oriented. PXRD data

collect data from millions of randomly oriented crystallite; therefore, it can provide strong and reliable diffraction intensities. The intensities and positions of the peaks are employed to identify the structure of the material. After the collection of the powder-diffraction pattern is performed, extraction of line intensities is performed by a variety of approaches methods; for instance, the Le Bail or Pawley approaches can be performed to search for structure models and sifted through to select plausible ones.

It must be remarked that the majority of nanoporous materials is synthesized in powder form, and thus, SXRD may not offer all kinetic information during the adsorption process, because the collection of a complete 3D data set from the single crystal is highly time-consuming compared to PXRD. Although PXRD provides accuracy in intensity measurements, it must be admitted that sometimes prediction structure with PXRD is challenging due to significant overlapping in the powder-diffraction patterns even for high-resolution data. In general, nanoporous materials possess relatively poor crystallinity, which renders the resolution of their structures barely possible from PXRD data. This problem is more significant in the case of nanocrystals featuring large unit-cell sizes and low symmetry. In such cases, a structureless pattern refinement of the experimental diffraction diagram gives the possibility to obtain the cell parameters as well as the space-group symmetry of these nanoporous materials.

As a representative example, Fig. 4 shows some examples of the structure of MCM-41, MCM-48, and MSM-50 by their PXRD.

Developing these ideas further, Fig. 5a shows the crystal structure of nanoporous Si-ZSM-5, as verified by XRD (Kokotailo et al. 1978).

Figure 5b illustrates the three-dimensional channels of the nanoporous ZSM-5 zeolite. The [−101], [011], and [101] reflections located at $2\theta = 7.92°$, 7.93°, and 8.01°, respectively, led to a total peak at ~8.0 (Hernández et al. 2018).

XRD also can be applied to specify the effect of modification on the structure of the nanoporous materials. For example, Fig. 6 illustrates the XRD result of a nanoporous LUS-1 silica samples before and after loading of TiO_2. The TiO_2-containing LUS-1 spectra show hexagonal symmetry with (100), (110), and (200) diffraction peaks

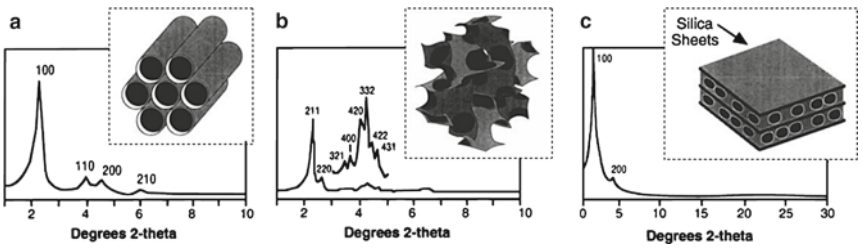

Fig. 4 XRD patterns and the assigned pore structures of **a** MCM-41 (hexagonal), **b** MCM-48 (cubic), and **c** MCM-50 (stabilized lamellar) (reproduced, with permission, from Barton et al. 1999)

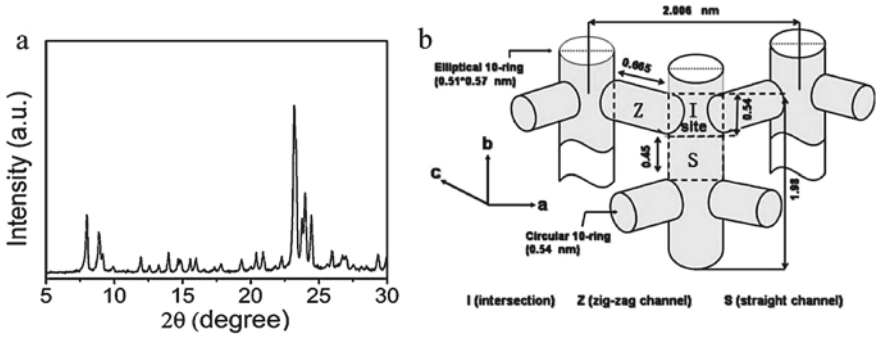

Fig. 5 Structure characterizations. **a** XRD pattern of nanoporous Si-ZSM-5, **b** A schematic illustration displaying the intrinsic microporous structure in a ZSM-5 crystal (reproduced, with permission, from Hernández et al. 2018)

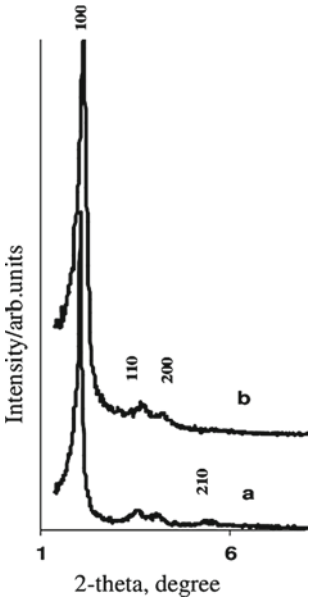

Fig. 6 XRD pattern of **a** LUS-1 nanoporous silica, **b** Ti/LUS-1 nanoporous silica (Badiei et al. 2009)

that assignable to hexagonal P6mm symmetry. The (100) peak demonstrates a well-defined mesostructure with a pore diameter of 2–50 nm. It was found from the XRD patterns the loading of TiO_2 on LUS-1 in solution did not have any effect on the order of the mesostructure (Badiei et al. 2009).

Many nanoporous materials are known to be electrical insulators, and their electron-beam sensitivity depends on the binding nature of the material. To overcome this challenge, more research is needed. Despite this weakness, the high-resolving power of electrons renders them very powerful for the characterization of nanoporous materials (Liu et al. 2013).

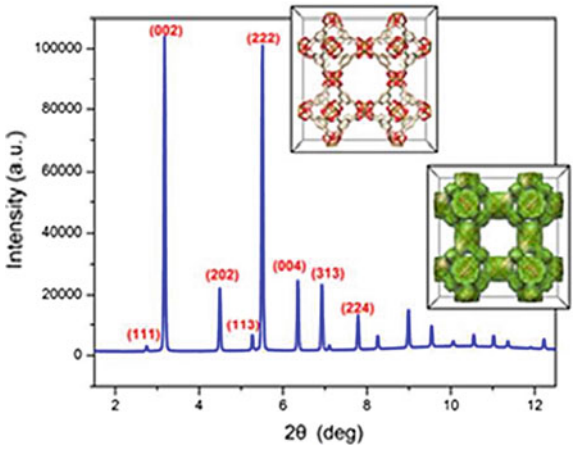

Fig. 7 Structure envelope generation using selected reflection (reproduced, with permission, from Chen et al. 2015)

Yakovenko et al. developed a method to characterize the structure envelope (SE) of a nanoporous MOF from either single-crystal or PXRD patterns (Yakovenko et al. 2013). To envelop the structure, the intensities of reflection were employed in SUPERFLIP software, to solve the structure of MOF, as shown in Fig. 7 (Chen et al. 2015).

However, in many cases, regardless of using the highest-quality powder-diffraction data sets, XRD fails to predict a good structure model. It frequently happens for nanoporous solids that often feature a 2D periodicity but exhibit no long-range order in the third dimension. Moreover, low electronic contrast, pore fillers with no or different periodicity, lamellar compounds, etc., provide an extra challenge in this regard. In a conclusion, to characterize structural transformations in the flexible structure of MOFs, incorporation of the gas adsorption with X-ray powder diffraction enables to determine and obtaining information about the mechanism and kinetics of "gate opening," swelling, and breathing which is significantly important for innovative materials design for future applications (Krause et al. 2016).

2.2 Electron Crystallography

In cases that the crystals are too small for characterizing by SXRD or the structures too complex for determining by PXRD, electron crystallography (EC) offers the best alternative tool for the structural determination of materials (Liu et al. 2013). By utilizing the diffracted electron beams in an electron, EC entails solving the crystal structure of a very small single crystal. Moreover, this method can probe smaller length-scale electrons due to their intrinsically smaller wavelengths vis-à-vis X-ray crystallography. Due to the much stronger interaction of the electron with matter compared to the X-ray, this technique gives the ability to study nano-sized crystals. In another word, X-ray powder sample reacts like a single crystal under electron beams.

Moreover, electrons are negatively charged, and they can be focused by electromagnetic lenses to form images. Indeed, EC is becoming a more common technique for the determination of unknown zeolites structure (Terasaki et al. 2004). High-resolution transmission electron microscopy (HR-TEM) images as a powerful technique can offer comprehensive information about atomic arrangements in a crystal, and it gives direct information about possible disorders.

The three-dimensional electron tomography (3DTEM) technique has been used to monitor some materials that possess composition variations on a nanoscopic scale in a non-periodic manner. This method has been applied to study biological systems (Anderson et al. 2004), but the applications to materials science more broadly are just beginning to be realized, with a great deal of promise.

Sakamoto et al. created a method that uses EC to predict 3D structures of mesoporous materials with disordered structures by use of high-resolution electron microscopy (HREM) (Sakamoto et al. 2000). By applying this technique, the 3D structure can solve at the nanoscale level, including the sizes and shapes of the pores and cages, their arrangements as well as their connectivity, as well as the sizes of openings. Their technique was developed particularly for periodic structural arrangements with mesoscale ordering and showed a good capability for characterizing a variety of mesoporous silica SBA structures.

Later, in 2013, electron diffraction was applied for the determination of the structure of a protein in 3D using a method called MicroED (Shi et al. 2013). MicroED is a cryoelectron microscopy (cryoEM) method that establishes the atomic resolution of structures from very small three-dimensional crystals (Shi et al. 2013). As such, this is a highly applicable technique if crystals can only be synthesized on a scale that is too small for analysis via X-rays (i.e., typically less than 1 μm) (Anderson et al. 2004). This allows for ready determination of crystals with particularly short crystal morphology, such as needle crystals, and also nanocrystals that are deliberately grown at a very small scale. Some structure solutions are shown in Fig. 8.

3 Oxidation State and Coordination

Detailed information about the oxidation station, coordination number, and interactions of adjacent compounds is essential in a composite material, as this allowed for optimization of material characteristics, which can trigger improved device performance. These factors sometimes change depending on the reaction conditions.

In nanoporous metal oxide, controlling these metal oxides with stable and tunable oxidation states, and coordination geometries are crucial for tailoring their catalytic, electronic, and optical properties. Local arrangements of atoms (coordination environment) are achieved by applying methods like X-ray absorption spectra (XAS)—Solid-state NMR—IR & Raman. For the oxidation state of nanoporous techniques included—X-ray photoelectron spectra (XPS), XAS—UV-Vis spectra are used.

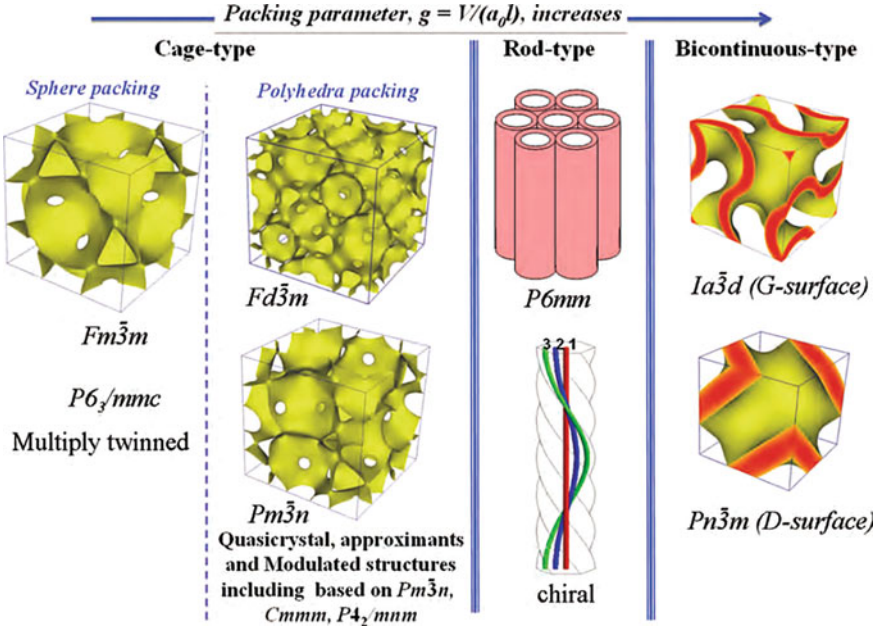

Fig. 8 Representative solved structure types of nanoporous materials via electron crystallography (reproduced, with permission, from Liu et al. 2013)

3.1 X-Ray Absorption Spectrum

X-ray absorption spectroscopy (XAS) is an enormously capable tool that provides information about the local structure around specific elements at the atomistic and molecular level (Koningsberger et al. 2000; Van Bekkum et al. 2001). X-ray absorption spectroscopy refers to experiments that the X-ray absorption coefficient $\mu(E)$ of the sample measures as a function of incoming energy (E) of the incident X-ray beam, in the vicinity of an absorption edge (at energy E_0) for one of the elements of the sample, denoted as the absorber.

Basic Principles of XAS

Passing a monochromatic beam of X-rays through a sample resulting partly scattered (diffracted) and partly absorbed (cf. Fig. 9a). Part of the incoming absorbed photons by atoms of the material causes a reduction in the intensity of the transmitted X-ray beam. Accordingly, the incident intensity I_0 will decrease depending on the absorption characteristics of the material. The Beer-Lambert Law (Eq. 2) is an empirical relationship between the absorption of X-rays to the properties of a matter that X-rays are passing through (Koningsberger et al. 2000).

$$I_t = I_0 \mathrm{e}^{-\mu(E)t} \tag{2}$$

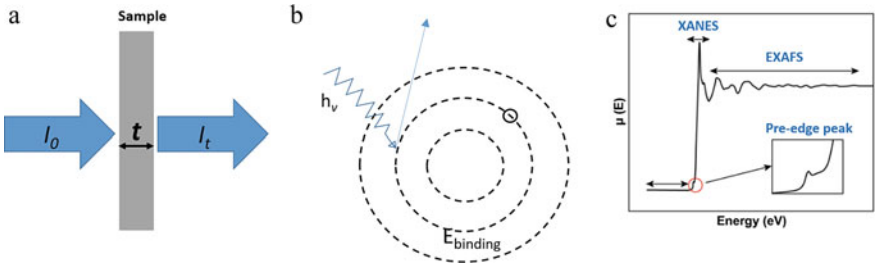

Fig. 9 **a** Schematic of the incident and transmitted X-ray beam, **b** Schematic of the photoelectric effect in terms of excitation of the different orbital, **c** Schematic of XAS including the pre-edge, XANES, and EXAFS regions

where $\mu(E)$ indicates the linear absorption coefficient, I_0 shows the incident X-ray intensity, I_t indicates the transmitted X-ray intensities, and t shows the thickness of the sample (Wang et al. 2019). When the binding energy of the core level is less than the energy of the incident X-ray, the electronic core level absorbs the X-ray (Van Oversteeg et al. 2017).

The flat area observed in Fig. 9c is for the situation that the incident X-ray energy is not sufficiently strong to excite the electrons to the highest unoccupied state or the vacuum and less than the binding energy of the electron in the element's orbital. Although, sometimes there are some unfavored transitions, including $1s$ to $3d$ in transition metals, which are indicated as a pre-edge peak (Fig. 9c). X-ray absorption near-edge structure (XANES) is called when the X-ray energy is strong enough to excite core electrons to the unoccupied state (the threshold energy or absorption edge), then X-ray is highly absorbed and leads to a sharp rise in the spectrum (Fig. 9c) (Martis 2011).

The XANES region is between 50 eV below the absorption edge toward 100 eV beyond the edge. As the spectrum is depending on the chemistry of the absorbing atom, thus, it is capable of extracting information for determining the oxidation state as well as the geometry of the element of interest. With further increase in X-ray energies, the area of the absorption spectra follows by the extended X-ray absorption fine structure (EXAFS), where expands into the range of thousands of eV beyond the absorption edge energy. The EXAFS function provides information on the next neighbor coordination shell of atoms; thus, information about the structure as well as the short-range environment of the X-ray absorbing atom can be achieved. The EXAFS function $\chi(E)$ is calculated from the:

$$\chi(E) = (\mu(E) - \mu_0(E))/\Delta\mu_0 \tag{3}$$

Here $\chi(E)$ represents the removal of X-ray absorption coefficient ($\mu(E)$) from background $\mu_0(E)$ and division by $\Delta\mu_o$ represents the normalization of the function.

To calculate $\chi(k)$ from the μ_{total} (experimentally acquired), a few steps are required to follow as shown in Fig. 10. The EXAFS function can be obtained from the absorption coefficients of the absorbing atom and the condensed phase:

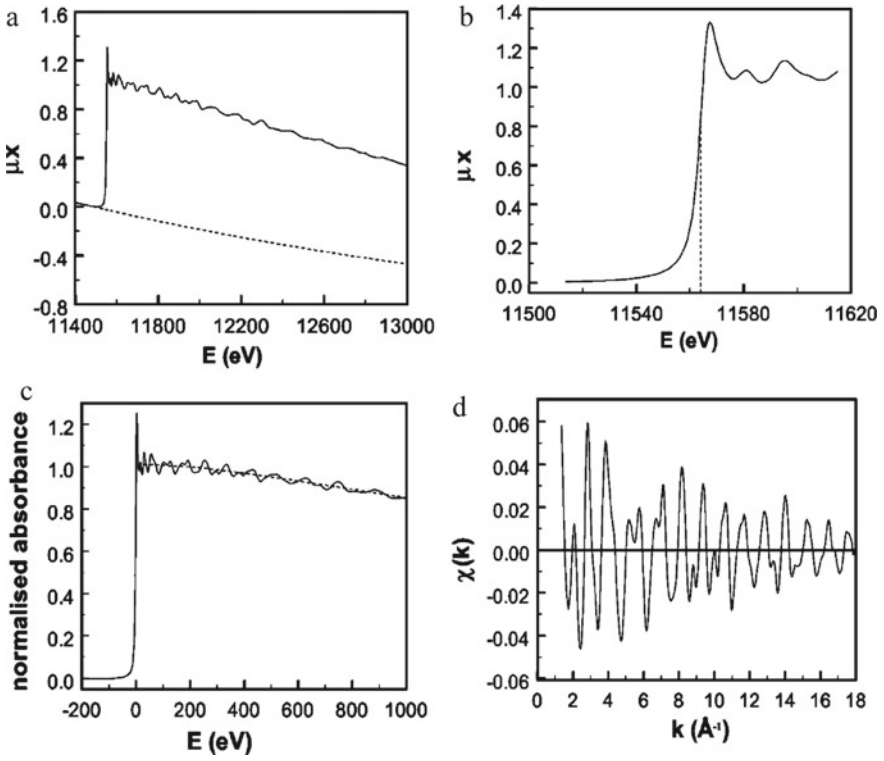

Fig. 10 Steps of extraction of the oscillatory part of an X-ray absorption spectrum for platinum foil: **a** removing the pre-edge background (- - -); **b** detecting the location of edge; **c** removing the post-edge background (- - -) and normalization; **d** transforming of the EXAFS spectrum to k scale through Eq. (4) after normalization (not displayed) (reproduced, with permission, from Koningsberger and Ramaker 2006)

$$\chi(k) = \sum_j \frac{N_j}{kR_j^2} \sin\left(2k \cdot R_j + 2\delta + \emptyset_j\right) \cdot \left|f_j(k)\right| \cdot \exp(-2\sigma_j^2 k^2) \cdot \exp\left(-\frac{2V_i R_j}{k}\right) \tag{4}$$

Here N_j is the average coordination number of the jth shell; R_j is the average interval between the absorbent atom and the jth shell; δ is the phase shift of emitting atom σ_j is the Debey-Waller factor, k is the photoelectron wave vector, $f_j(k)$ is the amplitude of the back-scattering factor of the jth neighboring atom, φ_j is the phase shift of back-scattering atom in jth shell, and V_i is the inelastic scattering of photoelectron wave. Information on the local molecular coordination environment can be achieved by analyzing the EXAFS data.

In the study done by *Sinfelt and Meitzner*, the X-ray absorption edge was employed to investigate the oxidation states of pre-cursors during different steps in the preparing

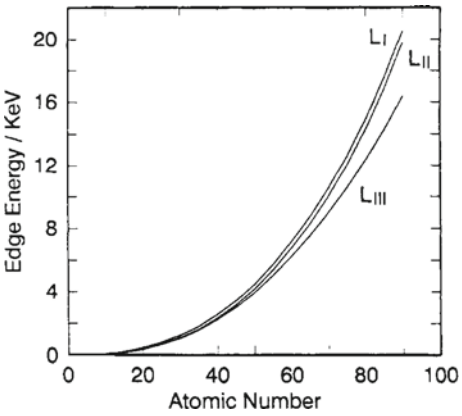

Fig. 11 L absorption edges energies of the elements as a function of atomic number (reproduced, with permission from Sinfelt and Meitzner 1993)

of a metal catalyst (Sinfelt and Meitzner 1993). Figure 11 indicates that in an absorption spectrum for each element, the absorption edges are observed at certain energies characteristic of the element. As shown in Fig. 11, the energies of the L_I edges (L_I edge is due to the excitation of electrons from 2s states) are more than L_{II} and L_{III} (L_{II} and L_{III} edges are due to the excitation of electrons from 2p states (Sinfelt and Meitzner 1993).

As mentioned earlier, the absorption edge position reveals the information about the oxidation state, whereas a higher oxidation state is resulting in a shift of the absorption edge to larger energy. As shown in Fig. 12, there is a linear correlation between the Co K-edge position and the Co oxidation state (Timoshenko and Cuenya 2021). Therefore, for finding the oxidation state for the new materials, an established relationship between the edge location and oxidation state for known reference materials can be employed. In Fig. 12, E_s corresponding to 80% of the total area under the pre-edge and near-edge for Co_3O_4 and E_r shows 80% of the total area under

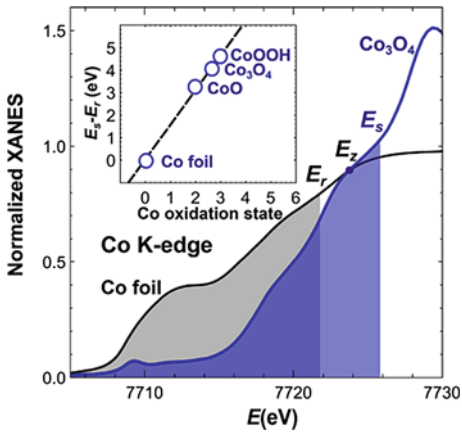

Fig. 12 Quantification of the shift between the absorption edge for metallic Co and Co_3O_4 (reproduced, with permission, from Timoshenko and Cuenya 2021)

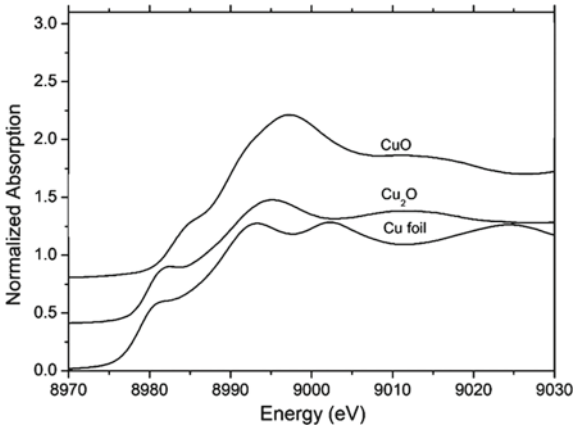

Fig. 13 Cu K-edge XANES spectra of Cu foil, CuO, and Cu_2O (Klaiphet et al. 2018)

the pre-edge and near-edge for Co foil, whereas E_z is referring to the point that Co foil spectrum crosses the of Co_3O_4 spectrum. Figure 12 displays a nearly linear relationship between $E_s - E_r$ and the Co oxidation state.

Figure 13 shows an example of a comparison of obtained XAS spectra from Cu foil (0 oxidation state), CuO (+2 oxidation state), and $CuCl_2$ (+2 oxidation state) (Klaiphet et al. 2018). As shown in this figure, the $\mu(E)$ of both Cu_2O and CuO at pre-edge is shifted to higher energies compared to Cu foil, which is expected based on their higher oxidation states.

3.2 X-Ray Photoelectron Spectrum

X-ray photoelectron (XPS) is a technique for the determination of the energy of photoelectrons released from the sample impacted by irradiating with X-rays. The measured kinetic energy of core electrons allows calculation of the binding energy of the ejected electron in the material. While the binding energy of the core electrons is unique to each element, any slight change in the binding energy of elements is dependent on the environment and oxidation state of the atom. Therefore, XPS is one of the most established and non-destructive methods for the determination of oxidation states (Alov 2005).

Principles of XPS

The relative positions of electronic energy levels and XPS Peaks are illustrated in Fig. 14. Generally, Mg Kα ($h\nu = 1253.6$ eV) or Al Kα ($h\nu = 1486.6$ eV) were applied as the X-ray light sources.

The kinetic energy (E_k) of the electron is express as:

$$E_k = h_\nu - BE - \phi \tag{5}$$

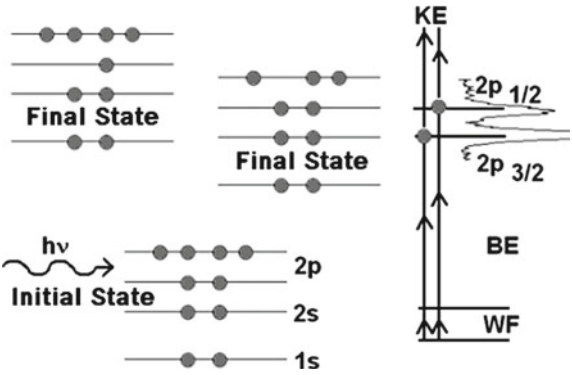

Fig. 14 Electronic energy levels and XPS peaks

where h is Planck's constant, ν is the frequency of the incident radiation, BE is the binding energy of the photoelectron, and ϕ is the work function (Son et al. 2020). When energy applies to the specimen, the electron excites and tends to depart from the nucleus and reaching the level that the binding energy of the nucleus is equal to the binding energy of the electron. The irradiated X-ray has high energy and is needed to emit the electrons of the K shell with considerable binding energy by the photoelectric effect (Fig. 14). As each element has its specified bonding energy, then analyzing the binding state of particular atomic orbitals of particular elements is feasible. Changing binding energy can be used to determine the oxidation state of the metal.

Lee et al. (2014) studied the porous properties of nanoporous manganese oxides. Among them, Mn_3O_4 and Mn_5O_8 exhibit similar textual properties including similar morphology, surface area, and crystal size of framework, but different oxidation states (Lee et al. 2014). Figure 15 shows the oxidation states of three nanoporous manganese samples (MnO, Mn_3O_4, and Mn_5O_8) determined by XPS. The Mn 3s XPS spectra revealed that the increase in the oxidation number of samples resulting in a gradual shift of the location of peak corresponded to the lower binding energy to the higher energy.

Along with subtracting background spectra, peaks from XPS are usually a combination of several smaller peaks, as shown in Fig. 15, so it is important to split the peaks (Raja and Barron 1934). This can be done with the software bundled with XPS equipment. Generally, the binding energy of each metal increases with a higher oxidation state.

Figure 16a shows a high-resolution Fe $2p_{3/2}$ XPS of a mixture of iron oxide powder with FeO (Fe^{2+}) and Fe_2O_3 (Fe^{3+}) (Wright and Barron 2017). The change in the oxidation state of the iron results in a shift in binding energy to higher levels. Another example is Cr_2O_3 $2p_{3/2}$, which appears as multiple peaks (Fig. 16b) (Wright and Barron 2017). Multiple peaks could also appear due to "charge-transfer satellites," from the sudden creation of a core-hole due to the XPS process.

Reference compounds of the metal with known oxidation states can be used to assist in the determination of oxidation states, from analysis of the peaks. For

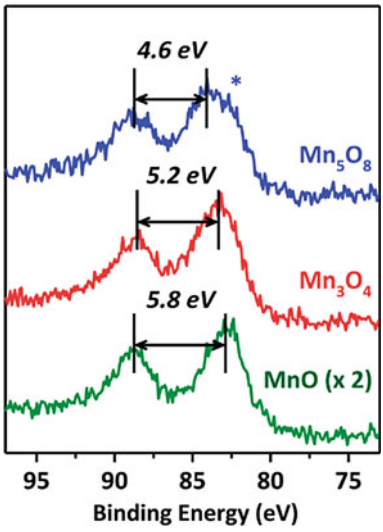

Fig. 15 Mn 3s XPS spectra of MnO, Mn_3O_4, and Mn_5O_8. The blue star shows the existence of low-valent (Mn^{2+}) manganese species in Mn_5O_8 (reproduced, with permission, from Lee et al. 2014)

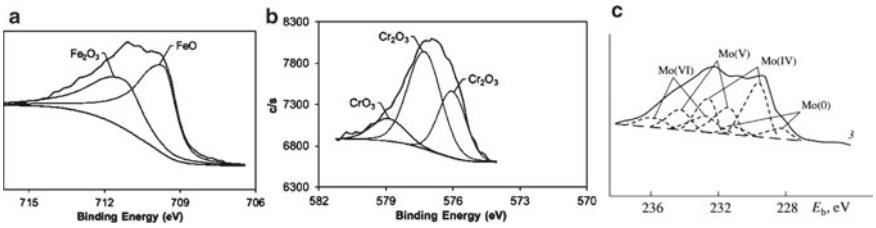

Fig. 16 **a** High-resolution Fe $2p_{3/2}$ XPS of mixed iron oxide powder, **b** High-resolution Cr $2p_{3/2}$ XPS peak for Cr_2O_3 showing an example of complex splitting, **c** Mo 3d XPS spectra of surface cleaned molybdenum crystals before (top solid line) and after (bottom dashed lines)

unknown vanadium oxide, for example, spectra of known vanadium oxides can be obtained and binding energies compare with the unknown. Moreover, the integration of the peaks can specify the relative amounts of each oxidation state.

The XPS database and binding energies of various metal complexes can be compared to those achieved in the *National Institute of Standards and Technology* (NIST).

However, there are some limitations in determining the oxidation state by XPS. The binding energy commonly increases with oxidation states, overlapping binding energy can happen for some compounds with the same metal but different oxidation states. For example, as illustrated in Table 1, $FeSO_4$ (Fe^{2+}) has a higher $2p_{3/2}$ binding energy than Fe_2O_3 (Fe^{3+}) *(*Raja and Barron 1934).

Table 1 Fe $2p_{3/2}$ XPS binding energy for various iron species

Species	Fe oxidation state	Fe $2p_{3/2}$ binding energy (eV)
Fe	0	706.3
FeO	2+	709.1
$FeSO_4$	2+	711.0
Fe_2O_3	3+	710.6

Even with limitations, XPS is a powerful technique that provides information on oxidation states materials including nanoporous materials.

3.3 UV–Vis Spectra

UV/Visible spectroscopy use to quantify the extinction (scatter + absorption) of light passing through a sample. This method is utilized to identify, characterize, and study nanomaterials, as these materials boast special properties which are sensitive to the size, shape, concentration, and refractive index near their surface. Because of its distinctive twin advantages, sporting inexpensive and facile analysis of substances, a UV-visible spectrometer is utilized in many disparate fields.

The UV radiation excites the electrons from the ground state to the state with a higher level of energy. The electromagnetic radiation between 190 and 800 nm and is divided into the range between the ultraviolet region (190–380 nm), and the visible region falls between 380 and 750 nm (Fig. 17).

To quantifying the sample's wavelength-dependent extinction spectrum, the intensity of UV/visible beam is quantified before and after passing through the sample and compared at each wavelength. By applying the Beer-Lambert Law, the absorption of spectra generated from these samples at given wavelengths can be related directly to the sample concentration. Indeed, the Beer-Lambert Law is based on the concept

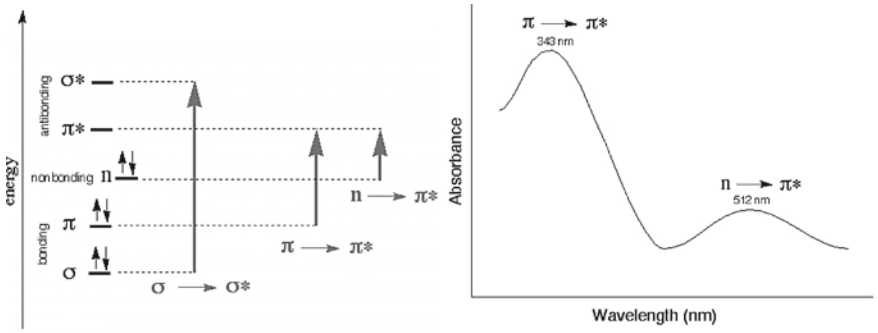

Fig. 17 ***n* to π^*** and ***π* to π^*** transitions occur in the UV-vis range, while ***σ* to σ^*** transition needs absorption of a photon with a wavelength out of UV-vis region

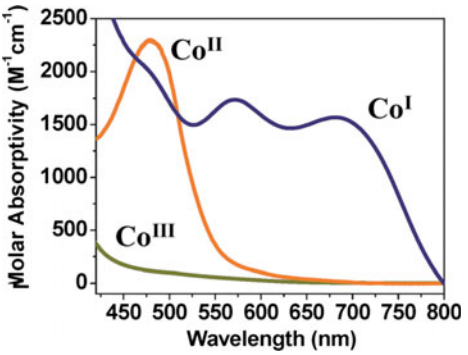

Fig. 18 UV-visible absorption spectra of 1 (Co^{III}) and its reduced Co^{II} analog with $\lambda = 480$ nm and Co^{I} analog with $\lambda = 572$ nm and $\lambda = 685$ nm (reproduced, with permission, from Basu et al. (2016)

that the larger the number of molecules able to absorb light of a specific wavelength, the larger the extent of light absorption. Indeed, in such a way, it is possible to access molecular structure and oxidation state via UV-VIS spectroscopy.

To illustrate this important concept, the UV-Vis applied for different oxidation states of e 3+, 2+, and 1+ oxidation states of the metal (Co) is illustrated in Fig. 18 (Basu et al. 2016).

3.4 Nuclear Magnetic Resonance (NMR)

To characterize nanoporous materials, even with using very high-quality powder-diffraction data sets, a traditional strategy such as X-ray fails in finding a good structure model for many cases (Taulelle et al. 2013). This limitation is more significant in the case of nanoporous solids, due to some of their properties, for example, some nanoporous have a 2D periodicity without order in the third dimension, low electronic contrast, pore fillers without or with various periodicities. Among the substitute strategies, nuclear magnetic resonance (NMR) crystallography is an important analytical method that offers an efficient way to determine the structure of nanoscale materials.

The phenomenon of NMR relies on the nuclei of atoms featuring magnetic properties which can be used to provide chemical information. In the NMR technique, when the nuclei that have non-zero spin located in a strong magnetic field, it creates a small energy difference between the spin-up and spin-down states. Physiochemical characteristics, such as structure, purity, and functionality, can be analyzed by this method. Recently, pulsed field-gradient NMR has been applied for evaluation of the diffusivity of nanomaterials, resulting in determining the size and species interaction. However, there are several disadvantages to this technique such as time-consuming and low detection sensitivity. Over the last decades, NMR has been widely used as a

non-destructive technique to characterize nanoporous materials featuring pore sizes from 1 to 100 nm.

The Basic Principle of NMR

A general Hamiltonian, H, describing the interactions experienced by a nucleus of spin I may be expressed as:

$$H = H_Z + H_D + H_{CS} + H_{SC} + H_Q \tag{6}$$

where H_Z: Zeeman interaction, H_D: dipolar interaction, H_{CS}: chemical shift, H_{SR}: spin-rotation interaction; H_Q: nuclear spin and quadruple (Table 2).

Therefore, the precise energy-level splitting is sensitive to some nuclear spin interactions, which are assessed by the physical and chemical properties of the nuclear spin system.

Owing to the sensitivity of changes in the coordination environment, this technique is applied as an element-specific structure-analyzing technique. Each of the nuclei in a crystal has its characteristics, such as the spin number, which can be 1/2 or more. When the number of measurable nuclei is larger, the number of possible one-dimensional (1D) and two-dimensional (2D) NMR experiments which can be obtained is much larger.

Solis state NMR (SsNMR) has been demonstrated as a complementing technique to diffraction techniques for determining the structure of nanoporous materials.

The environments of framework atoms of porous materials can investigate by the NMR spectroscopy of ^{29}Si, ^{27}Al, ^{31}P, ^{69} Ga, or ^{71} Ga nuclei, or ^{1}H, ^{7}Li, ^{23}Na nuclei that are charge-compensating ions. These measurements can give information about the number of inequivalent atomic sites as well as the multiplicity of these sites. Some recent developments in NMR are the ability to probe inter-nuclear distances, increase the power of NMR (Taulelle et al. 2013).

Taulelle and coworkers studied the application of NMR crystallography for nanoporous materials (Taulelle et al. 2013). They (Taulelle et al. 2013) showed that the use of NMR data associated with diffraction methods and modeling can provide systematic ways to achieve the structure models. This is especially important for the structure determination of the complex nanoporous crystals.

1D collection of data can provide different structural information. From the isotropic chemical shifts, information such as the nature of the neighboring atom and the coordination number of the atom can be achieved. For instance, ^{7}Al in 4-, 5-

Table 2 Approximate range of different spin interaction (in Hz) (NMR Interactions 2020)

Zeeman	10^8
Dipolar	10^3
Chemical Shift	10^3
Scalar Coupling	10
Quadrupolar	10^6

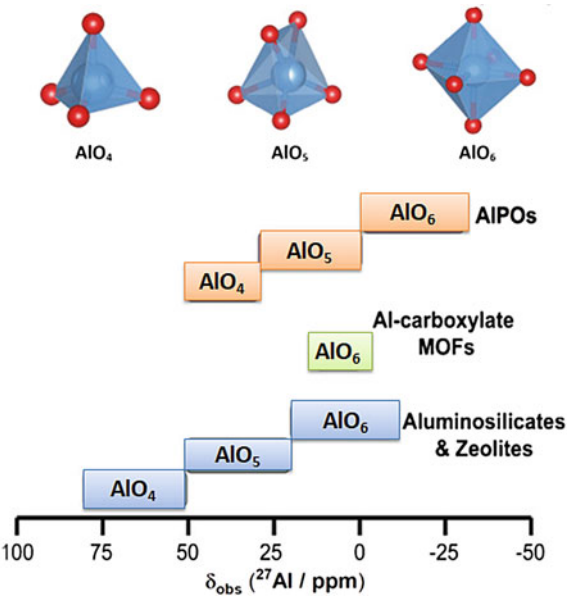

Fig. 19 ^{27}Al chemical shift variation in most types of porous solid

or 6-fold coordinated (Fig. 19), or ^{13}Cin 2-, 3- or 4-coordination state (hybridization sp, sp^2, sp^3), or the environment of SiO_4 in Q^4, Q^3, Q^2, Q^1, Q^0 environments (n of Qn refers to the number of bridged oxygen atoms in the first coordination sphere of the Si atom) can be determined as 1D ^{27}Al, ^{13}C and ^{29}Si MAS NMR spectra, respectively (Taulelle et al. 2013).

Wen et al. using NMR in both 1D and 2D to investigate the electrochemical redox activity between V^{5+} and V^{2+} oxidation states (Wen et al. 2019). Solid-state 2D ^{27}Al 3Q-MAS and 1D ^{27}Al single-pulse NMR spectrum obtained from precipitation of reaction between V_2O_5 and Al_2Cl_7 (cf. Fig. 20a, b, respectively). The ^{27}Al single-pulse NMR spectrum showed that the precipitate contains aluminum moieties for three different coordination environments: Al^{IV} (~85 ppm), Al^{V} (~34 ppm), and Al^{VI} (~4 ppm). The 2D ^{27}Al 3Q-MAS spectrum correlates the MAS dimension (horizontal) with an isotropic dimension (vertical). The 1D slices of the different Al coordination environments are shown in Fig. 20c.

Another example to emphasize the determination of oxidation state from NMR is shown in Fig. 21. ^{31}P MAS NMR spectrum was obtained to determine the oxidation state of phosphorus. Two peaks at −10 (A_1) and −6 (A_2) ppm indicated two non-equivalent positions of the phosphine present in the framework. Another peak was shown at 35 ppm is corresponding to oxidized phosphine (B). A phosphine fraction of 85% was observed for the peak area of combining A_1 and A_2 compared to the peak area of B (Morel et al. 2015).

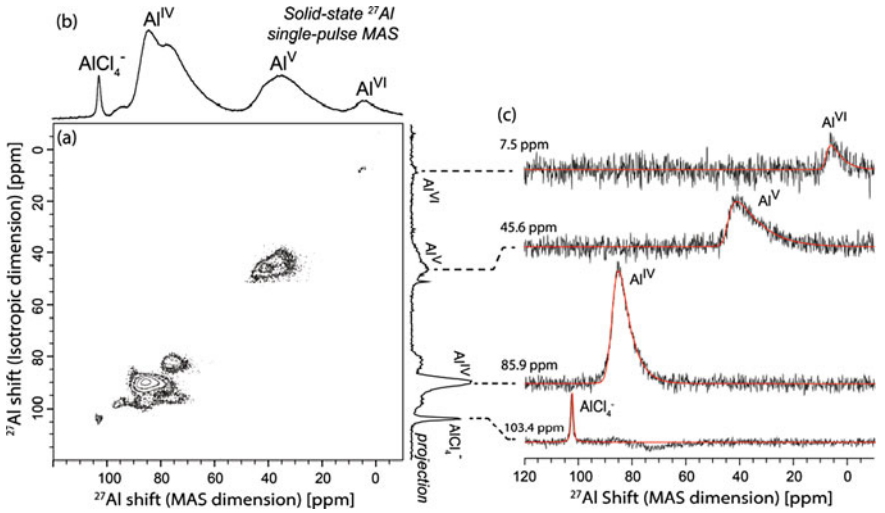

Fig. 20 **a** SsNMR of 2D ^{27}Al triple-quantum (3Q)-MAS NMR spectra. **b** A separately acquired quantitative 1D ^{27}Al single-pulse MAS spectrum is displayed, where ^{27}Al signals associated with 4-, 5-, and 6-coordinated Al moieties are labeled. **c** 1D slices of different Al coordination environments (reproduced, with permission, from Wen et al. 2019)

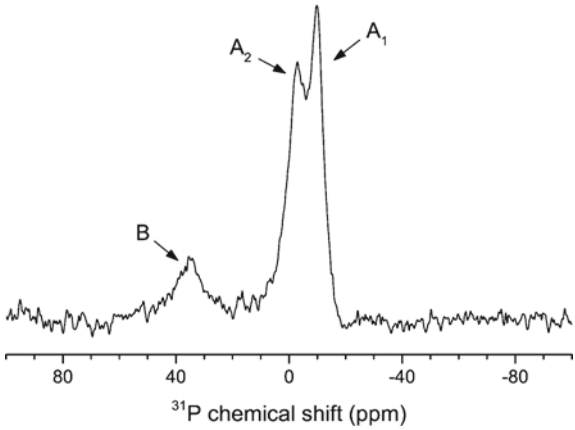

Fig. 21 ^{31}P MAS NMR spectra (right) of LSK-15. NMR signals are labeled according to phosphorus oxidation state (with permission from Morel et al. 2015)

4 Chemical Composition

The chemical composition of nanoporous materials can be determined by elemental analysis techniques, including inductively coupled plasma-atomic emission spectroscopy ICP-AES and energy dispersive X-Ray spectroscopy (EDX).

ICP-AES is an emission-based spectrophotometric method to detect more than 70 elements with a concentration range of ppb to ppm. ICP-AES employs the fact that

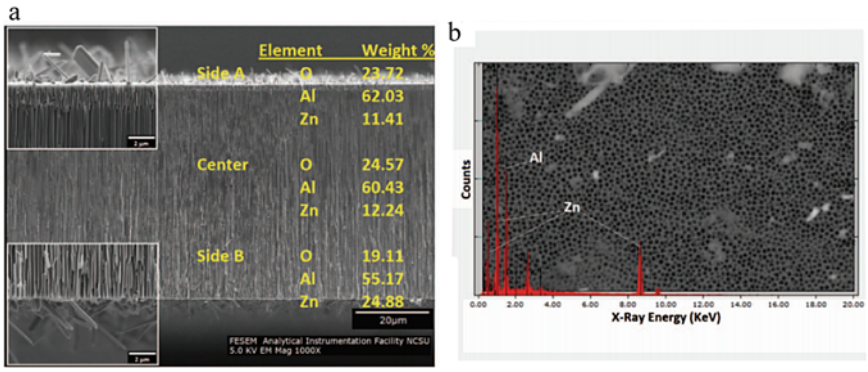

Fig. 22 **a** Cross-section view of a 20 nm nanoporous anodized aluminum oxide with an 8 nm ZnO coating membrane, showing the crystals present on the surface. **b** EDX spectrum obtained from the 200 nm circular pore side, showing Al and Zn peaks (reproduced, with permission, from Petrochenko et al. 2013)

when excited electrons return to the ground state, they emit energy at a given wavelength. Every element emits energy at unique wavelengths particular to its chemical character and ICP-AES select a single or a very few wavelengths for a given element (Ghodke 2015). By determining the emitted wavelengths and their intensities (with intensity proportional to concentration), this technique can determine the elemental composition of the sample. This technique can analyze all elements, except argon.

The elements present in the nanoporous materials can be identified by applying EDX analysis (Zhao et al. 2019). EDX technique incorporates with imaging tools such as scanning electron microscopy (SEM) and transmission electron microscopy (TEM) can detect the elemental composition of the imaged area. The data provided by EDX analysis contain spectra presenting peaks corresponding to making up the composition of the analyzed sample.

As an example, Fig. 22b shows an EDX spectrum of a nanoporous ZnO-coated anodized aluminum-oxide membrane (Petrochenko et al. 2013). Distinguished Zn and Al peaks were observed on spectra that were acquired from the membrane (Petrochenko et al. 2013).

A comparison between elemental analysis performed by CP-AES for Phosphotungstates (MPW) and EDX is presented in Table 3 (Ghodke 2015).

5 Pore Analysis

The gas-sorption analysis is among the most useful experimental techniques for structural characteristics of open porous solids such as specific and external surface area, total and micropore volume of nanoporous materials (Thommes and Schlumberger 2021). Generally, gas-sorption probes the interaction between gas and the sample,

Table 3 Elemental analysis by ICP-AES and EDX

Materials	% by ICP-AES analysis			% by EDX analysis (atomic %)			
	M (IV)	P	W	M (IV)	P	W	O
ZrPW	Zr = 26.88	4.96	25.37	Zr = 6.79	18.53	20.67	–
TiPW	Ti = 14.84	4.64	24.97	Ti = 46.61	37.99	15.40	–
SnPW	Sn = 36.82	4.67	29.41	Sn = 59.33	23.31	17.37	–
12-TPA/ZrO_2-20	Zr = 58.62	0.09	16.48	Zr = 28.75	0.11	3.44	67.70
12-TPA/TiO_2-20	Ti = 46.76	0.08	16.17	Ti = 28.63	0.15	0.88	70.34
12-TPA/SnO_2-20	Sn = 60.01	0.08	18.04	Sn = 18.40	0.12	2.57	78.92

From Ghodke 2015, with permission

this can happen in microporous or mesoporous adsorption, also in monolayer and multilayer adsorption (Keshavarz et al. 2021). Brunauer, Emmett, and Teller (BET) are the most popular method based on physical adsorption of a gas on the adsorbent surface for the determination of the specific surface area of porous materials. The BET isotherm is applicable for a sample covered by more than one layer of gas molecules:

$$\frac{P}{P_0} = \frac{1}{a_m C} + \frac{p_0(C-1)}{a_m C} \tag{7}$$

where P_0 is the tension of saturated vapor at a particular temperature, a_m is the specific monolayer capacity (mol/g), and the parameter C is a constant including adsorption and condensation heat (Širc et al. 2012).

The adsorption isotherm represents the dependency of the adsorbed gas on pressure at a constant temperature. The specific surface area can be measured according to

$$A_{\text{sp}}(\text{BET}) = N_A.a_m.\sigma \tag{8}$$

where A_{SP} (BET) is the BET specific surface area of adsorbent, N_A is the Avogadro constant, and σ is the area of the sample occupied by the adsorbate in the monolayer.

The original derivation of the BET relation is based on the assumption that a statistical multilayer coverage of a non-microporous surface (Reichenauer 2011). BET theory assumes the interactions between neighbor adsorbed molecules just happen in a vertical direction. Another assumption of this theory is that the adsorption energy is not dependent on the type of the adsorption sites (Sing et al. 1985; Lowell 2004).

The Barrett, Joyner, and Halenda (BJH) method which is based on the Kelvin equation (which relates the pressure to pore size) is the most widespread method to calculate the pore volume and pore size distribution in a mesoporous solid (Barrett and Halenda 1951). BJH theory assumes that the shape of the pore is cylindrical.

It was shown that the BJH method for narrow mesopores (pore diameter < 10 nm) underestimates pore size by approximately 20–30% (Thommes et al. 2015). This error can be minimized by applying methods based on molecular simulation or density-functional theory (DFT) software which is applicable for different types of pore geometries.

Advanced statistical thermodynamics models, including DFT, molecular dynamics (MD), and Monte Carlo (MC) simulations, yield a molecular-level acquaintance of adsorption in pores and apply to characterize nanoporous materials. A nonlocal density-functional rheory (NLDFT) approach is a precise method that is offered for the characterization of nanoporous materials. The NLDFT has been established to predict the adsorption/desorption isotherms in nanopores of various geometries with pore diameters about 0.3–100 nm (Reichenauer 2011). The results of pore-size distributions of mesoporous calculating from the NLDFT method are in good agreement with other techniques applied for characterization of pore structure (transmission electron microscopy and X-ray diffraction).

The International Union of Pure and Applied Chemistry (IUPAC) recommended the classification of isotherms regarding physical-adsorption characterization that is shown in Fig. 23. Based on their classifications: Pores are typically microporous which yield to Type I isotherms; nonporous or pores with diameters exceeding micropores adsorbents give Type II isotherm; Type III and V isotherms observed when there are small adsorbent-adsorbate interactions potential and are associated with a pore diameter in the range of 1.5–100 nm; Type IV isotherms represent mesoporous

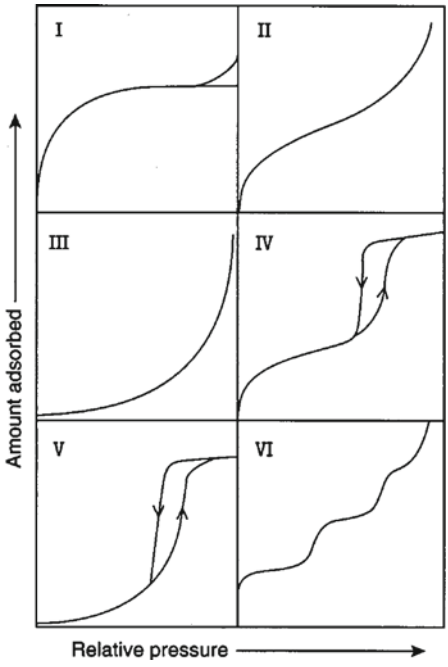

Fig. 23 Classification of adsorption isotherms (reproduced, with permission, from Barton et al. 1999)

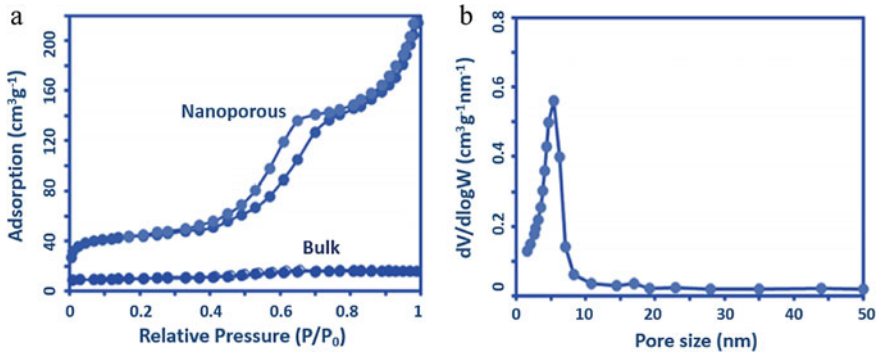

Fig. 24 **a** N_2 adsorption-desorption isotherms of the balk and nanoporous $NiMoO_4$ samples, **b** BJH pore-size distribution plot of the nanoporous $NiMoO_4$

materials; and Type VI isotherms indicate layer-by-layer adsorption on a nonporous surface. The suitable selection of the adsorption isotherm, along with the proper pore-size calculation such as molecular simulation or DFT, allows the possibility to evaluate precisely the pore-size distribution within the porous material.

As an example for this section, the N_2 adsorption-desorption isotherms, as well as the BJH pore-size distribution for nanoporous and bulk NiMoO4, are illustrated in Fig. 24 (Moosavifard et al. 2014). As shown in Fig. 24a, the nano-cast sample has a type IV isotherm that is characteristic of nanoporous or mesoporous materials, while the bulk sample has a type II isotherm representing nonporous or macroporous materials. Moreover, the pore-size distribution of nanoporous $NiMoO_4$ calculated by BJH (Fig. 24b) shows a uniform pore-size distribution. Then their sample showed a high-ordered nanoporous structure with narrow pore-size distribution and large surface area.

Determination of pore sizes and pore-size distributions from N_2 isotherms of some nanoporous materials like microporous polymers suffer from an absence of proper models. As shown in Fig. 25b, the acquired results from the same isotherm were compared by the NLDFT and Horvarth–Kawazoe (HK) analysis, which are two predominant methods. Although both models are based on the same assumption, significant differences between the models are evident.

Using nitrogen in gas-sorption experiments has a certain drawback in comparison to noble gases such as Argon: it experiences a stronger interaction with polar moieties of polymers because of its quadruple moment. Moreover, it is possible that some of the pores are not occupied by nitrogen due to the relatively large size of nitrogen. Despite these limitations, nitrogen sorption is the most used technique for the analysis of nanoporous materials mostly due to its accessibility in many laboratories. Recently, the use of carbon dioxide as an adsorbent to characterize ultra-micropores has become more common in the analysis of microporous materials. This method is well known for analyzing activated carbons.

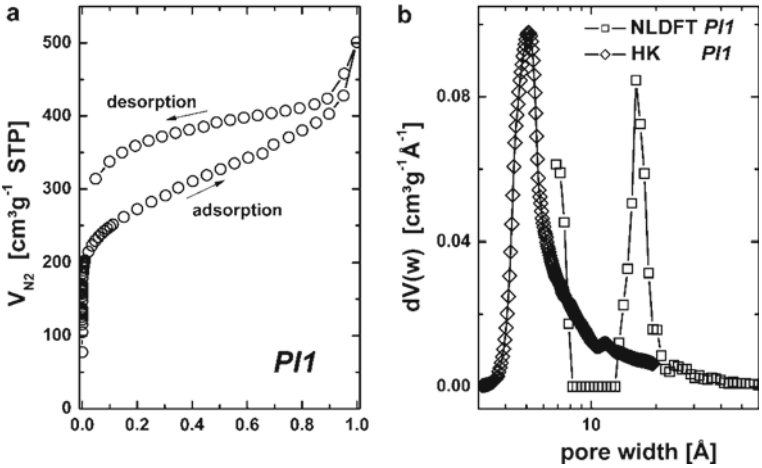

Fig. 25 **a** Nitrogen sorption isotherm of a spirobiuorene-based polyimide network. **b** Comparison of the micropore analysis data obtained from the HK and NLDFT model (Weber et al. 2008, with permission)

6 Morphology: SEM

Scanning electron microscope (SEM) is a very common technique for observing and quantifying the shape, surface texture, and particle distribution of materials and provides information about morphology, topography, composition, and crystallography of materials, including nanoporous materials. This imaging technique allows for direct visualization and investigation of nanoporous materials with advanced structures. Due to high resolution along with a deep depth of focus, SEM is considered a powerful visualization tool for nanostructures analysis, including nanoporous materials. Recent progress in the resolution of SEM and the large depth of field allows for the capture of the microstructures of the sample with three-dimensional information. Therefore, analysis of SEM images has highlighted attention in the nanostructured world, especially in nanoporous materials, as the complex networks between the pores and the walls appear vividly under an SEM. The structure of various places of the nanoporous sample can be visualized directly by SEM. Therefore, so-obtained images from SEM enable useful and important details to compare the local structures with the whole sample and are considered as an alternative to observing pores.

Applying a method developed by Zhou & Qiao through a large number of SEM images were used to provide detailed structural information such as 2D pore and wall size, fractal dimension, and porosity (Zhao and Qiao 2016). This method for SEM-image polishing (SIP), according to the quantitative SEM-image analysis (QSIA) technique for nanoporous materials, provides the possibility of fast and accurate data mining at the nanoscale in nanoporous materials. However, the lack of structural

information is one of the foundational difficulties in allowing for quantitative image analysis.

The Basic Principle of SEM

In an SEM, a high-energy beam is emitted from electrons that interact with atoms on the surface of the specimen or near it. The resolution attained by SEM is mainly dependent upon the operating parameters (around 1 nm). To prevent a repulsive reaction of an electron beam, the surface of a non-conductive sample is usually coated with a very thin layer of gold or platinum. However, the sputter coating can lead to removing the atomic number-contrast and elemental composition analysis.

The depth of field (Δf) defines as the distance within which the sample remains in acceptable focus which depends on two factors including magnification (M) and the beam convergence (α_0):

$$\Delta f \approx \frac{0.2\,\text{mm}}{M\alpha_0} \tag{9}$$

where the factor of 0.2 mm is regarding the resolution of the human eye over the SEM images.

Figures 26a–c illustrates that the three-dimensional pore structure of the nanoporous polyethylene was analyzed by SEM.

SEM images provide images of the sample with information about surface defects like cracks, etching residues, depressions, differential swelling, and perforations. However, there are some drawbacks of SEM, such as degradation of the sample, which alters or destroys details and consequently changes results and conclusions. Moreover, there is the possibility of damage to the sample by the SEM's electron beam. In addition, SEM is not able to image wet samples, due to possible damage

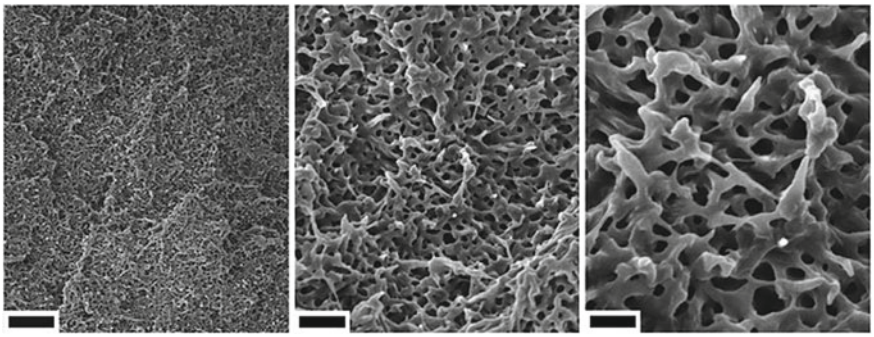

Fig. 26 Morphology of a bicontinuous microemulsion-derived, nanoporous polyethylene using SEM, two right images are a higher-magnification view of the central part of the area illustrated in the left image. The scale bars from left to right: 3 μm, 750 nm, and 300 nm, respectively (Jones and Lodge 2012, with permission)

during vacuum required during operation. Another limitation of SEM is when applied to capture measurement involving height or process color image.

7 Pore Structure: TEM

Transmission electron microscopy (TEM) is considered the most widely used technique in characterizing nanomaterials, due to its sub-nanometer resolution and the capability of directly observing very small pore structure. The image of nanomaterials provided by TEM at a resolution of atomic dimensions ranging from ~100 nm to single atom size. This method has the ability of imaging a variety of nanostructures such as nanoporous materials. The highly detailed images provide valuable insight into structural information including particle size and morphology and high-resolution images of the framework at an atomic level.

Similar to SEM, imaging the non-conductive samples is challenging for TEM; therefore, for some metal oxides before imaging, covering the sample with a thin layer of gold is recommended. One disadvantage of TEM is the difficulty in preparing the samples since the grids for the sample holder are very tiny, and the sample must be sufficiently small (100 nm thin) or a very fine powder. However, the methods of preparing the sample for TEM might change the underlying pore size and pore structure.

Recently, this technique has encountered very promising breakthrough progress in the aberration correction for atomic-level imaging, the cryogenic TEM for imaging biological specimens, and the new in situ instrumentation. Excitingly, in situ TEM started to be a prevailing technique to observe reactions at the nanoscale level. TEM boasts providing high temporal and spatial resolution, as well as direct visualization of any changes in structural, morphological, or elemental distribution at the nanoscale which considered as an advantage of this method compared with other in situ techniques such as scanning-tunneling microscopy (STM), atomic force microscopy (AFM), and various X-ray methods.

TEM images of nanoporous materials include micropores pore (size < 2 nm), mesoporous (2–50 nm), and macrospores (size > 50 nm) with examples are shown in Fig. 27 (Fayed et al. 2016, with permission).

TEM offers more advantages compared to SEM to provide spatial resolution in high-quality and analytical measurements. Moreover, by utilizing TEM, it is possible to visualize the internal connectivity. TEM images offering instant feedback and consequently allowing control during the nanopore drilling processes.

To glean a better comparison between two imaging technologies for nanoporous materials, Fig. 28 shows the SEM and TEM of nanoporous manganese oxides (Lee et al. 2014).

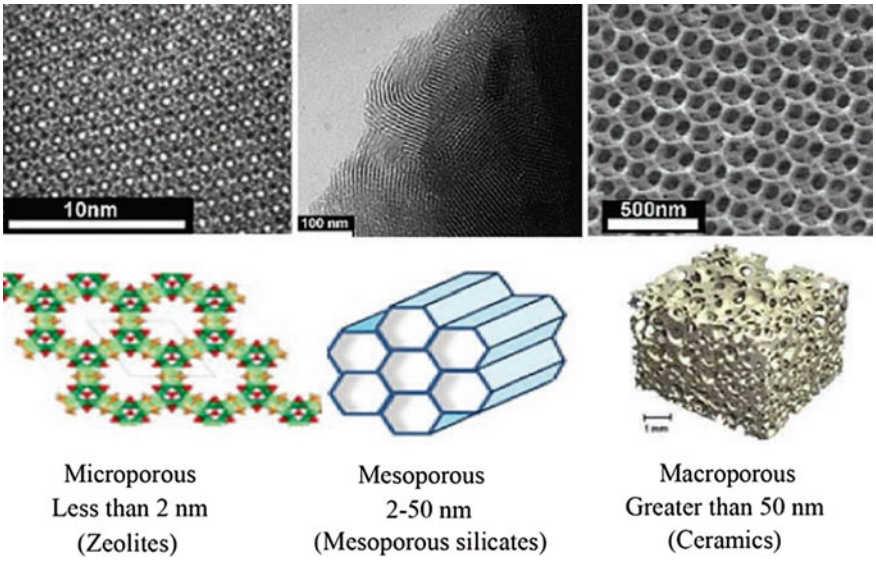

Fig. 27 Three categories of nanoporous materials and their TEM images (Fayed et al. 2016, with permission)

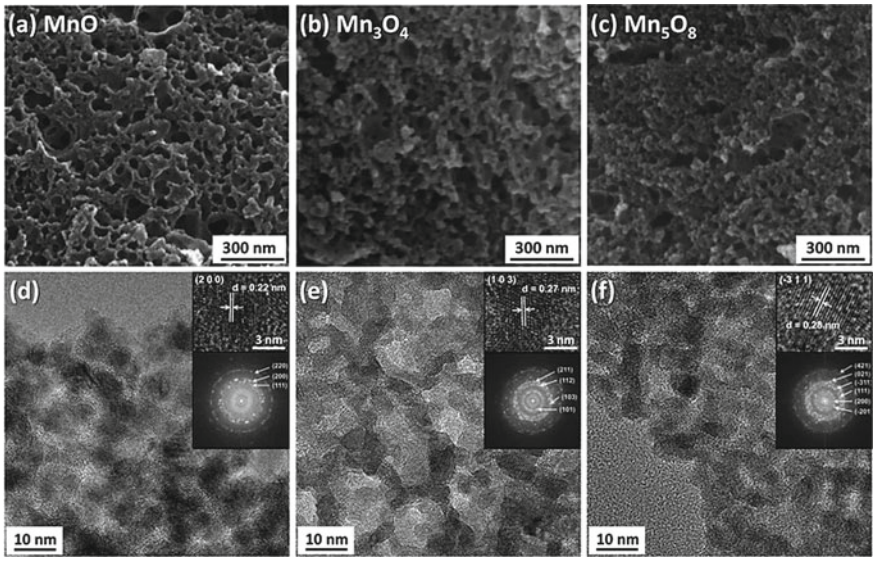

Fig. 28 Comparing the SEM images (**a**–**c**) and TEM images (**d**–**f**) of converted manganese oxides. (**d**–**f**, inserts) HR-TEM images of nanoporous MnO (**a**, **d**), Mn_3O_4 (**b**, **e**), and Mn_5O_8 (**c**, **f**) (Lee et al., 2014, with permission)

8 Conclusions

Comprehensive knowledge of the structural properties including pore size and connectivity can assist to improve the efficiency of nanoporous materials in a disparate different fields, such as, *inter alia*, gas storage, separation, and catalytic processes. From this perspective, huge advances have been done recently regarding the physisorption characterization of nanoporous materials. The IUPAC technical report in 2015 outlined their suggestions for the surface and pore-size analysis.

Structural and morphological characterization for nanoporous materials can obtain by various techniques including X-ray diffraction techniques, electron crystallography, small-angle X-ray, gas adsorption, and neutron scattering, together with mercury porosimetry, scanning electron microscopy, and transmission electron microscopy, as well as nuclear magnetic resonance (NMR) methods. The oxidation state and coordination properties can be analyzed adopting UV-Vis, X-ray absorption spectroscopy, NMR, etc. Inductively coupled plasma mass spectrometry (ICP-MS), energy dispersive analysis of X-rays (EDAX), and X-ray photoelectron spectroscopy (XPS) are generally using for elemental analysis of nanoporous materials. Evaluation of surface area and pore size is performed by N_2 adsorption-desorption isotherm. Each of these methods has advantages, disadvantages as well as a limited application range.

One important future direction in nano- and porous-materials analysis lies in the use of molecular simulation as an important method to accompany experimental materials characterization. Using both empirical-potential models and electronic-structure methods allows for the simulation of atomic- and nanoscale defects and surface/bulk features, and the extraction of spectroscopy results therefrom, which can then be compared with experimentally. However, excitingly, this approach can be used for predictive materials design as a prototyping tool in nanomaterials discovery. In such a way, we can determine desirable spectral features from molecular simulation and "tune" material properties, such as defects and nanoscale geometry features, to arrive at an optimal porous-materials design.

References

Alov, N.V.: Determination of the states of oxidation of metals in thin oxide films by X-ray photoelectron spectroscopy. J. Anal. Chem. **60**(5), 431–435 (2005). https://doi.org/10.1007/s10809-005-0114-x

Anderson, M.W., Ohsuna, T., Sakamoto, Y., Liu, Z., Carlsson, A., Terasaki, O.: Modern microscopy methods for the structural study of porous materials. Chem. Commun. **4**(8), 907–916 (2004). https://doi.org/10.1039/b313208k

Badiei, A., Gholami, J., Khaniani, Y.: Synthesis and characterization of titanium supported on high order nanoporous silica and application for direct oxidation of Benzene to Phenol. E-J. Chem. **6**(Suppl. 1), 324–329 (2009). https://doi.org/10.1155/2009/292483

Barrett, E.P., Joyner, L.G., Halenda, P.P.: The determination of pore volume and area distributions in porous substances. I. Computations from nitrogen isotherms. J. Am. Chem. Soc. **73**(1), 373–380

Barton, T.J., Bull, L.M., Klemperer, W.G., Loy, D.A., McEnaney, B., Misono, M., Monson, P.A., et al.: Tailored porous materials. Chem. Mater. **11**(10), 2633–2656 (1999). https://doi.org/10.1021/cm9805929

Basu, D., Mazumder, S., Niklas, J., Baydoun, H., Wanniarachchi, D., Shi, X., Staples, R.J., Oleg Poluektov, H., Schlegel, B., Verani, C.N.: Evaluation of the coordination preferences and catalytic pathways of heteroaxial cobalt oximes towards hydrogen generation. Chem. Sci. **7**(5), 3264–3278 (2016). https://doi.org/10.1039/c5sc04214c

Bragg, P.W.H., Bragg, W.L.: The reflexion of X-rays by crystals. Proc. r. Soc. Lond. a. **88**(605), 428–438 (1913)

Chen, Y.P., Liu, Y., Liu, D., Bosch, M., Zhou, H.C.: Direct measurement of adsorbed gas redistribution in metal-organic frameworks. J. Am. Chem. Soc. **137**(8), 2919–2930 (2015). https://doi.org/10.1021/ja5103579

Fayed, T.A., Shaaban, M.H., El-Nahass, M.N., Hassan, F.M.: Hybrid organic-inorganic mesoporous silicates as optical nanosensor for toxic metals detection. Int. J. Chem. Appl. Biol. Sci. **1**(2), 1–18 (2016)

Ghodke, U.C., Shrinivas: A comparative study on catalytic activity of solid acid catalysts towards microwave assisted synthesis of coumarin derivatives. Int. J. Sci. Res. (IJSR) **4**(1), 1933–1939 (2015). https://www.ijsr.net/archive/v4i1/SUB15710.pdf

Halder, G.J., Kepert, C.J.: In situ single-crystal X-ray diffraction studies of desorption and sorption in a flexible nanoporous molecular framework material. J. Am. Chem. Soc. **127**(21), 7891–7900 (2005). https://doi.org/10.1021/ja042420k

Helliwell, M., Helliwell, J.R., Logar, N.Z., Mali, G., Tušar, N.N., Kaučič, V.: Structure characterisation of nanoporous materials using state-of-the-art single-crystal X-ray and neutron diffraction techniques. Acta Chim. Slov. **55**(4), 709–718 (2008)

Hernández, M.A., Abbaspourrad, A., Petranovskii, V., Rojas, F., Portillo, R., Salgado, M.A., Hernández, G., de los Angeles Velazco, M., Ayala, E., Quiroz, K.F.: Estimation of nanoporosity of ZSM-5 zeolites as estimation of nanoporosity of ZSM-5 zeolites as hierarchical materials. In: Zeolites and Their Applications Size, pp. 73–90. https://doi.org/10.5772/intechopen.73624

Jones, B.H., Lodge, T.P.: Nanocasting nanoporous inorganic and organic materials from polymeric bicontinuous microemulsion templates. Polym. J. **44**(2), 131–146 (2012). https://doi.org/10.1038/pj.2011.136

Kaskel, S. (2017). The chemistry of metal-organic frameworks: synthesis, characterization, and applications. Johnson Matthey Technol. Rev. **61**. https://doi.org/10.1595/205651317X695091

Keshavarz, L., Ghaani, M.R., Don MacElroy, J.M., English, N.J.: A comprehensive review on the application of aerogels in CO_2-adsorption: materials and characterisation. Chem. Eng. J. **412**, 128604 (2021). https://doi.org/10.1016/j.cej.2021.128604

Klaiphet, K., Saisopa, T., Pokapanich, W., Tangsukworakhun, S., Songsiriritthigul, C., Saiyasombat, C., Céolin, D., Songsiriritthigul, P.: Structural study of Cu(II): glycine solution by X-ray absorption spectroscopy. J. Phys.: Conf. Ser. **1144**(1) (2018). https://doi.org/10.1088/1742-6596/1144/1/012063

Kokotailo, G.T., Lawton, S.L., Olson, D.H., Meier, W.M.: Structure of synthetic zeolite ZSM-5. Nature (1978). https://doi.org/10.1038/272437a0

Koningsberger, D.C., Ramaker, D.E.: Applications of X-ray absorption spectroscopy in heterogeneous catalysis: EXAFS, atomic XAFS and delta XANES. In: Chapter 3.1.3.2 Structure and Morphology, pp. 774–803 (2006)

Koningsberger, D.C., Mojet, B.L., Van Dorssen, G.E., Ramaker, D.E.: XAFS spectroscopy; fundamental principles and data analysis. Top. Catal. **10**(3–4), 143–155 (2000). https://doi.org/10.1023/a:1019105310221

Krause, S., Bon, V., Senkovska, I., Stoeck, U., Wallacher, D., Többens, D.M., Zander, S., et al.: A pressure-amplifying framework material with negative gas adsorption transitions. Nature **532**(7599), 348–352 (2016). https://doi.org/10.1038/nature17430

Lee, J.H., Sa, Y.J., Kim, T.K., Moon, H.R., Joo, S.H.: A transformative route to nanoporous manganese oxides of controlled oxidation states with identical textural properties. J. Mater. Chem. A **2**(27), 10435–10443 (2014). https://doi.org/10.1039/c4ta01272k

Liu, Z., Fujita, N., Miyasaka, K., Han, L., Stevens, S.M., Suga, M., Asahina, S., et al.: A review of fine structures of nanoporous materials as evidenced by microscopic methods. J. Electron Microscopy **62**(1), 109–146 (2013). https://doi.org/10.1093/jmicro/dfs098

Lowell, S.: Characterization of Porous Solids and Powders: Surface Area, Pore Size and Density. Edited by LLC SPRINGER SCIENCE+BUSINESS MEDIA. Kluwer Academic Publishers (2004)

Martis, M.: In Situ and Ex Situ Characterization Studies of Transition Metal Containing Nanoporous Catalysts, pp. 1–216 (2011). http://discovery.ucl.ac.uk/1334587/

Moosavifard, S.E., Shamsi, J., Fani, S., Kadkhodazade, S.: 3D Ordered Nanoporous NiMoO4 for high-performance supercapacitor electrode materials. RSC Adv. **4**(94), 52555–52561 (2014). https://doi.org/10.1039/c4ra09118c

Morel, F.L., Pin, S., Huthwelker, T., Ranocchiari, M., Van Bokhoven, J.A.: Phosphine and phosphine oxide groups in metal-organic frameworks detected by P K-Edge XAS. Phys. Chem. Chem. Phys. **17**(5), 3326–3331 (2015). https://doi.org/10.1039/c4cp05151c

NMR Interactions (2020, August 15). Retrieved September 10, 2021, from https://chem.libretexts.org/@go/page/1823

Petrochenko, P.E., Skoog, S.A., Zhang, Q., Comstock, D.J., Elam, J.W., Goering, P.L., Narayan, R.J.: Cytotoxicity of cultured macrophages exposed to antimicrobial zinc oxide (ZnO) coatings on nanoporous aluminum oxide membranes. Biomatter **3**(3) (2013). https://doi.org/10.4161/biom.25528

Raja, P.M.V., Barron, A.R.: Physical methods in chemistry. Nature **134**(3384), 366–367 (1934). https://doi.org/10.1002/jctb.5000533702

Reichenauer, G.: Structural characterization of aerogels. Aerogels Handbook (2011). https://doi.org/10.1007/978-1-4419-7589-8

Sakamoto, Y., Kaneda, M., Terasaki, O., Zhao, D.Y., Kim, J.M., Stucky, G., Shin, H.J., Ryoo, R.: Direct imaging of the pores and cages of three-dimensional mesoporous materials. Nature **408**(6811), 449–453 (2000). https://doi.org/10.1038/35044040

Senthil Kumar, P., Grace Pavithra, K., Naushad, M.: Characterization techniques for nanomaterials. In: Nanomaterials for Solar Cell Applications. Elsevier Inc. (2019). https://doi.org/10.1016/B978-0-12-813337-8.00004-7

Shi, D., Nannenga, B.L., Iadanza, M.G., Gonen, T.: Three-dimensional electron crystallography of protein microcrystals. Elife **2**, 1–17 (2013). https://doi.org/10.7554/elife.01345

Sinfelt, J.H., Meitzner, G.D.: X-ray absorption edge studies of the electronic structure of metal catalysts. Acc. Chem. Res. **26**(1), 1–6 (1993). https://doi.org/10.1021/ar00025a001

Sing, K.S.W., Everett, D.H., Haul, R.A.W., Moscou, L., Pierotti, R.A., Rouquérol, J., Siemieniewska, T.: Reporting physisorption data for gas/solid systems with special reference to the determination of surface area and porosity. Pure Appl. Chem. **57**(4), 603–619 (1985). https://doi.org/10.1515/iupac.57.0007

Širc, J., Hobzová, R., Kostina, N., Munzarová, M., Juklíčková, M., Lhotka, M., Kubinová, Š., Zajícová, A., Michálek, J.: Morphological characterization of nanofibers: methods and application in practice. J. Nanomater. 2012 (2012). https://doi.org/10.1155/2012/327369

Son, D., Sanghoscho@kist re kr Cho, Nam, J., Lee, H., Kim, M.: X-ray-based spectroscopic techniques for characterization of polymer nanocomposite materials at a molecular level. Polymers **12**(5) (2020). https://doi.org/10.3390/POLYM12051053

Taulelle, F., Bouchevreau, B., Martineau, C.: NMR crystallography driven structure determination: nanoporous materials. CrystEngComm **15**(43), 8613–8622 (2013). https://doi.org/10.1039/c3ce41178h

Terasaki, O., Ohsuna, T., Liu, Z., Sakamoto, Y., Garcia-Bennett, A.E.: Structural study of mesoporous materials by electron microscopy. Stud. Surf. Sci. Catal. **148**, 261–288 (2004). https://doi.org/10.1016/s0167-2991(04)80201-5

Thommes, M., Schlumberger, C.: Characterization of nanoporous materials. Annu. Rev. Chem. Biomol. Eng. **12**(5), 5.1–5.23 (2021). https://doi.org/10.1201/9781420082753-c6

Thommes, M., Kaneko, K., Neimark, A.V., Olivier, J.P., Rouquerol, F.-R., Sing, K.S.W.: Physisorption of gases, with special reference to the evaluation of surface area and pore size distribution. Pure Appl. Chem. **87**, 1051–1069 (2015). https://doi.org/10.1515/pac-2014-1117

Timoshenko, J., Cuenya, B.R.: In situ/operando electrocatalyst characterization by X-ray absorption spectroscopy. Chem. Rev. **121**(2), 882–961 (2021). https://doi.org/10.1021/acs.chemrev.0c00396

Van Bekkum, H., Flanigen, E.M., Jacobs, P.A., Jansen, J.C.: Introduction to Zeolite Science and Practice: Preface 1st Edition. Studies in Surface Science and Catalysis, vol. 137 (2001)

Van Oversteeg, C.H.M., Doan, H.Q., De Groot, F.M.F., Cuk, T.: In situ X-ray absorption spectroscopy of transition metal based water oxidation catalysts. Chem. Soc. Rev. **46**(1), 102–125 (2017). https://doi.org/10.1039/c6cs00230g

Wang, M., Árnadóttir, L., Xu, Z.J., Feng, Z.: In situ X-ray absorption spectroscopy studies of nanoscale electrocatalysts. Nano-Micro Lett. **11**(1), 1–18 (2019). https://doi.org/10.1007/s40820-019-0277-x

Weber, J., Antonietti, M., Thomas, A.: Microporous networks of high-performance polymers: elastic deformations and gas sorption properties. Macromolecules **41**(8), 2880–2885 (2008). https://doi.org/10.1021/ma702495r

Wen, X., Liu, Y., Jadhav, A., Zhang, J., Borchardt, D., Shi, J., Wong, B.M., Sanyal, B., Messinger, R.J., Guo, J.: Materials compatibility in rechargeable aluminum batteries: chemical and electrochemical properties between vanadium pentoxide and chloroaluminate ionic liquids. Chem. Mater. **31**(18), 7238–7247 (2019). https://doi.org/10.1021/acs.chemmater.9b01556

Wright, K., Barron, A.: Catalyst residue and oxygen species inhibition of the formation of hexahapto-metal complexes of group 6 metals on single-walled carbon nanotubes. J. Carbon Res. **3**(4), 17 (2017). https://doi.org/10.3390/c3020017

Yakovenko, A.A., Reibenspies, J.H., Bhuvanesh, N., Zhou, H.C.: Generation and applications of structure envelopes for porous metal-organic frameworks. J. Appl. Crystallogr. **46**(2), 346–353 (2013). https://doi.org/10.1107/S0021889812050935

Zhao, C., Qiao, Y.: Characterization of nanoporous structures: from three dimensions to two dimensions. Nanoscale **8**(40), 17658–17664. https://doi.org/10.1039/c6nr05862k

Zhao, C., Zhang, Y., Wang, C.C., Hou, M., Li, A.: Recent progress in instrumental techniques for architectural heritage materials. Heritage Sci. **7**(1), 1–50 (2019). https://doi.org/10.1186/s40494-019-0280-z